DECAY DYNAMICS IN MOLECULAR BEAMS

Klavs Hansen*[1,2]
[1]*Department of Physics, School of Science, Center for Joint Quantum Studies, Tianjin University, 92 Weijin Road, 300072, Tianjin, China*
[2]*Department of Physics, University of Gothenburg, 41296, Gothenburg, Sweden*

Received 22 January 2020; accepted 7 April 2020

Published online in Wiley Online Library (wileyonlinelibrary.com). DOI 10.1002/mas.21630

The phenomenon of power law decays in molecular beams is reviewed. The transition from a canonical to a microcanonical description of the decay is analyzed, and the appearance of the power law decay derived. Deviations from a power law often contain information on parallel competing processes. This is illustrated with examples where thermal radiation or dark unimolecular channels are the competing processes. Also corrections to the power law due to finite heat capacities and from nonideal energy distributions are derived. Finally, the consequences for the interpretation of action spectroscopy data are reviewed. © 2020 The Authors. Mass Spectrometry Reviews published by Wiley Periodicals, Inc. Mass Spec Rev

Keywords: *unimolecular reactions; clusters; power law decay; equilibration times*

I. INTRODUCTION

Molecular beams represent the cleanest method to study the structure of molecules and clusters due to the absence of interactions with substrates, which will unavoidably modify the properties of deposited particles, often in less than perfectly understood ways. For clusters, molecular beam studies are of particular importance because these species are thermodynamically unstable and must be produced on the spot where they are investigated. Both reasons have rendered molecular beam studies extremely important for cluster science, in spite of the fact that a number of applications are aimed at the use of deposited clusters, with catalysis as a prime example (Ishida et al., 2020). The power of molecular beam studies has been demonstrated by the discoveries of shell structures, both of the geometric packing type (Echt, Sattler, & Recknagel, 1981), of electronic shell structure (Knight et al., 1984; Katakuse et al., 1985), and of the fullerenes (Kroto et al., 1985).

Molecular beams come with some special features when it concerns the thermal behavior of both clusters and molecules. The principal reason is that the components of molecular beams are decoupled from the thermalizing heat bath that is necessary to describe a system as canonical. Although the production of clusters can often be described in terms of canonical equilibrium or quasi-equilibrium processes, once the particles leave the region of production and move into the ultrahigh vacuum sector of a molecular beam device, contact to the environment is reduced to a very occasional, and usually destructive, collision with a residual gas molecule.

Systematic studies of these special molecular beam features have produced diagnostic tools for a range of thermal phenomena of clusters. The purpose of this review is to describe how the special beam features arise and how they find applications in thermally activated unimolecular decays, including emission of electrons and photons in thermal processes.

These aspects are by now well established experimentally, primarily by work at ion storage rings (Andersen et al., 1996, 2001; Hansen et al., 2001; Tomita et al., 2001; Andersen et al., 2003a; Andersen, Heber, & Zajfman, 2004; Fedor et al., 2005; Toker et al., 2007; Froese et al., 2011; Lange et al., 2012; Toker et al., 2012; Martin et al., 2013; Menk et al., 2014; Martin et al., 2015; Breitenfeldt et al., 2016; Hansen et al., 2017b; Ji et al., 2017; Martin et al., 2017; Anderson et al., 2018; Bernard et al., 2019; Martin et al., 2019), occasionally in a form where other channels are present, but also at single pass devices such as time-of-flight mass spectrometers (Hansen & Campbell, 1996; Hansen & Echt, 1997; Ferrari et al., 2015; Hansen et al., 2017a; Ferrari et al., 2018a, b), and here the focus will be on the theoretical aspects.

The remainder of the paper contains a detailed discussion of the exponential decay frequently considered a paradigm for thermal decays, and demonstrate that there are significant limits to its applicability. This is followed by a derivation of decay rates for hot systems (molecules, clusters and nanoparticles) in vacuum, which introduces the $1/t$ dependence. The following section analyzes cases where corrections to the leading order $1/t$ decay rate are needed and provides those. After this, a section describes the effect of dark competing channels, and the paper ends with a description of the consequences for the analysis of action spectroscopy data.

II. LIMITS OF EXPONENTIAL DECAY

The exponential decay is a standard representation of statistical decays of quantal and thermal nature in both physics and chemistry. In spite of its frequent use, it applies only to a very special class of situations. Exponential functions represent decay

*Correspondence to: Klavs Hansen, Department of Physics, School of Science, Center for Joint Quantum Studies, Tianjin University, 92 Weijin Road, 300072 Tianjin, China. E-mail: klavshansen@tju.edu.cn
*Dedicated to Professor Einar Uggerud.

rates when systems (molecules, nuclei, etc.) decay out of a single state or, more generally, out of a collection of states with the same decay constant. The situation is realized in the decay of nuclei that disintegrate by the weak nuclear interactions from some very long-lived state which is effectively an eigenstate of the Hamiltonian describing the system (Pais, 1988). This is perhaps the simplest manifestation of the decay of a single state.

Also thermally activated processes may proceed exponentially, although the setting is very different from that of nuclear disintegration. Chemical reactions that proceed over an energy barrier in thermal processes have rates that depend strongly on the internal energy present in the reacting systems. This very well-known fact is reflected in the theories of unimolecular reactions that have been developed during the last century, and it is the basis of the empirical relationship between reaction rate constants and the temperature that was proposed by Arrhenius more than a century ago (Arrhenius, 1889).

For thermally activated processes, an exponentially decaying state requires an ensemble of molecules with an internal energy distribution that is independent of time, apart from the exponentially decreasing overall amplitude. For gas phase systems such distributions may be maintained by intermolecular collisions. Radiative equilibration is possible and can be included on an equal footing with collisions in the description, although only a few examples of a dominating radiative equilibration mechanism that lead to complete equilibrium distributions have been reported so far for lab experiments (O'Connor et al., 2016; Schmidt et al., 2017). As an energy source for beams, absorption of ambient radiation provides an important mechanism for dissociation of loosely bound molecules and clusters on long time scales, see e.g. (Niedner-Schatteburg & Bondybey, 2000; Dunbar, 2004; Rahinov et al., 2016). The phenomenon is known as blackbody infrared radiative dissociation (BIRD).

This mechanism and collisional (re-)equilibration both have the potential to ensure that decays will not completely deplete the high energy tail of the distribution, which is the part of the distribution from which the decays occur. Re-equilibration will cause the balance between depletion and repopulation to reach a steady state, which will make the decay exponential. The single quantum state of the nuclear decay is then replaced by the entire thermal, time invariant excitation energy distribution, which acts as, and indeed is, a single decaying state in thermal decays.

An obvious question for the quantitative description of unimolecular decays in a *nominally* canonical thermal equilibrium is what requirements must be fulfilled by the re-equilibration process to ensure that a decay can be represented by the rate constants pertaining to an *actual* canonical equilibrium. Specifically, what values must a re-equilibration rate constant take to make the canonical energy distribution relevant for calculating rate constants? As this question is closely related to the question of the decay rates in the limit of no equilibration, this will first be examined.

The gas phase unimolecular reactions that will be considered here can be described as

$$A \rightarrow B + C, \tag{1}$$

with a rate constant which depends on the excitation energy, E, of A:

$$k = k(E). \tag{2}$$

Rotational degrees of freedom can be disregarded for the present purpose. The species B, C can be molecules, atoms or electrons. Their precise nature is irrelevant for the considerations that follow here, as long as the reaction is thermally activated, i.e., that it requires that some subset of the internal degrees of freedom are elevated above a threshold, E_a, for the reaction to proceed.

In canonical thermal equilibrium at temperature T, the distribution of excitation energies in the reactant species A is given by its vibrational level density (density of states) $\rho(E)$, as

$$P_e(E)\mathrm{d}E = \frac{\rho(E)\mathrm{e}^{-E/T}}{Z}\mathrm{d}E, \tag{3}$$

where Z is the canonical partition function:

$$Z = \int_0^\infty \rho(E)\mathrm{e}^{-E/T}\mathrm{d}E. \tag{4}$$

Boltzmann's constant is set to unity, which is simply a choice of unit system. Energies and temperatures are measured in identical units, and heat capacities and entropies are dimensionless.

For any process that occurs with a rate constant significantly below the collision frequency in the gas, the reaction will be of activated nature and will occur predominantly from the high energy tail of the distribution of Equation (3) due to the strong energy dependence of the k in Equation (2) in this type of reactions. The Arrhenius formula pertains to such energy distributions. To see how the formula appears, represent the involved rate constant in terms of the level densities of the reactant, $\rho(E)$, and the product, $\rho_p(E)$, as

$$k(E) \approx \omega\frac{\rho_p(E - E_a)}{\rho(E)}, \tag{5}$$

with ω a frequency factor, and E_a the activation energy of the process. The appearance of the ratio of level densities in this rate constant follows from detailed balance. See e.g., Weisskopf, 1937; Brink & Stringari, 1990; Hansen, 2018b, where also examples of the detailed balance expression for ω can be found. Here it will set to a constant. These matters are discussed at length in chapter 5 of Hansen (2018b) to which the interested reader is referred for more details. The salient point here is that a number of details provided by more accurate theories of unimolecular decay rates will not appear in the ensemble averages that are the core of the material presented here, and it would be misleading to elaborate on such details. A number of different, relevant corrections to the expression are discussed below, though (see Eq. (35) and the text following that), and will be included after the theoretical baseline has been established.

For the schematic level densities

$$\rho(E) \propto E^s, \tag{6}$$

corresponding to $s + 1$ classical harmonic oscillators, the rate constant becomes

$$k(E) = \omega\left(\frac{E - E_a}{E}\right)^s, \tag{7}$$

This is close to a realistic description of thermionic emission rate constants where the number of vibrational degrees does not change during the process, and this very simple expression allows to focus on the essential points, although it should be stressed again that Equation (7) does not apply as a universally valid description of all aspects of unimolecular decays.

The rate constant for an equilibrium energy distribution is given by

$$k(T) = \int_0^\infty k(E) P_e(E) \mathrm{d}E. \tag{8}$$

(The same symbol is used for both the rate constant as a function of temperature and of energy, but this abuse of notation should not cause any confusion.) With Equation (5) and the expression for the population, the rate constant is calculated to

$$\begin{aligned} k(T) &= \int_0^\infty \omega \frac{\rho_p(E - E_a)}{\rho(E)} \frac{\rho(E) \mathrm{e}^{-E/T}}{Z} \mathrm{d}E \\ &= \int_0^\infty \omega \rho_p(E - E_a) \frac{\mathrm{e}^{-E/T}}{Z} \mathrm{d}E \\ &= \omega \frac{Z_p}{Z} \mathrm{e}^{-E_a/T}, \end{aligned} \tag{9}$$

where Z_p is the product partition function. Both partition functions in the expression refer to the internal degrees of freedom. For systems where the thermal excitations are carried predominantly by vibrations and where the geometric averages of the vibrational frequencies of precursor and product are the same, $\overline{\omega}$, their ratio is equal to

$$\frac{Z_p}{Z} = \left(\frac{\hbar \overline{\omega}}{T} \right)^3 \tag{10}$$

in the classical (high temperature) limit. At lower temperatures the ratio is closer to unity. In either case, the variation with energy is relatively slow, and whether or not one wants to include this into ω or not is partly a matter of taste. Apart from these qualifications, Equation (9) is the Arrhenius formula.

In the absence of a re-equilibration mechanism, the decay will proceed in time by slowly eroding the high energy end of the distribution in Equation (3). The energy distributions at some measurement time, t, defined as the time elapsed after the ensemble has been created, will then be given by

$$P(E; t)\mathrm{d}E = \frac{\rho(E) \mathrm{e}^{-E/T}}{Z} \mathrm{e}^{-k(E)t} \mathrm{d}E. \tag{11}$$

Figure 1 shows the energy distributions, initially generated with a temperature of 1500 K, that remain after $t = 1$ µs, 1 ms, and 1 s, for a molecule decaying with the schematic rate constant given by

$$k(E) = 10^{15} \mathrm{s}^{-1} \left(\frac{E - 3\,\mathrm{eV}}{E} \right)^{20}, \tag{12}$$

corresponding to the expressions in Equations (5) and (6) for 21 harmonic oscillators. The depletion shown in Figure 1 leads to an approximate power law decay with a power of −0.89 in this model case, as illustrated in Figure 2. The precise value of the power is influenced by the initial energy distribution, a question that will be discussed in detail below, but the nonexponential decay is a robust feature of this and similar situations.

Adding a re-equilibration mechanism to the energy distributions in Figure 1 provides a continuous repopulation of the high energy, decaying parts of the distribution. With a simple description of the (re-)equilibration it can be modeled as a reshuffling of the energy distribution with a rate constant denoted k_e. A realistic description is considerably more involved and is the topic of active research (King & Barker, 2019; Lendvay & Schatz, 2019; Robertson, 2019), but the simple description used here will make the point. Including

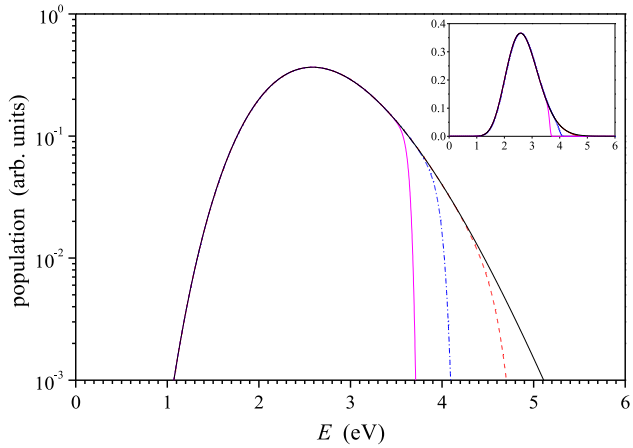

FIGURE 1. The canonical energy distribution at time zero (black, full line), and as depleted at $t = 1$ µs (red, dashed line), 1 ms (blue, dash-dotted line), and 1 s (magenta, full line). The decayed fractions are 0.4%, 3%, and 7% at the three times mentioned. The inset shows the same data on a linear scale. [Color figure can be viewed at wileyonlinelibrary.com].

the depletion due to the energy dependent reaction rate constant gives a time development for the energy distribution $P_s(E; t)$ of

$$\frac{\mathrm{d}P_s(E; t)}{\mathrm{d}t} = -k(E)P_s(E; t) - k_e(P_s(E; t) - P_e(E; t)), \tag{13}$$

where the time dependence of the equilibrium distribution P_e amounts to a time dependent normalization constant. Normalization of P_e to the same value as P_s ensures conservation of mass in the re-equilibration process.

Figure 3 shows the numerically calculated temporal development of the ensemble average rate constant of the model system for three values of the equilibration constant, k_e, and identical values of all other parameters. Note that the quantity plotted is the average rate constant in the remaining population versus time, and not the population nor the decay rate. The horizontal sections of the curves thus represent exponential decays. As the ensembles generated at different times by Equation (13) are not those of

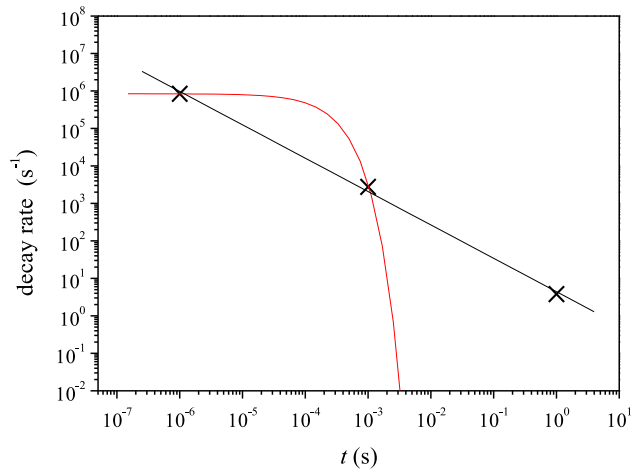

FIGURE 2. The decay rates calculated with Equation (11) at 1 µs, 1 ms, and 1 s, corresponding to the distributions shown in Figure 1. The strongly bending, red curve is the exponential decay fitted from the first two points (note the double-logarithmic scale). The straight line is a fit of a power law with the exponent −0.89. [Color figure can be viewed at wileyonlinelibrary.com].

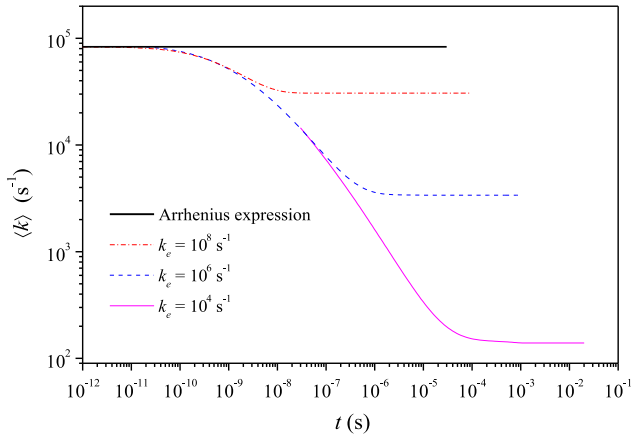

FIGURE 3. Ensemble averages of the rate constants in simulated energy distributions with the three re-equilibration constants given in the frame and the rate constant given in Equation (7). Horizontal lines correspond to exponential decays. The bold horizontal line just below 10^5 s^{-1} is the Arrhenius decay constant. The simulations were terminated when 5% of the initial abundance was left. The bulk parts of the decays occurs during the exponential decay phases. [Color figure can be viewed at wileyonlinelibrary.com].

thermal equilibrium, the average rate constant is also not the thermal average, i.e., $\langle k \rangle \neq k(T)$.

Two features are immediately noted from the curves. The first is that there is a long transient before the exponential decay is established, and that the duration of this depends strongly on the value of k_e. The second is that the measured rate constants, given by the plateaus at long times, also depend strongly on the value of k_e. The two observations are clearly related; the smaller the re-equilibration rate, the later in time the steady state will appear and the smaller therefore also the observed exponential decay constant. At very short time, the curves coincide with the Arrhenius value $k(T) = \omega \exp(-E_a/T)$, as expected, because no decay has taken place and the energy distributions are still canonical.

To describe the long time horizontal parts of the curve where decays are observed to be exponential, a stationary energy distribution state with an overall exponential decay can be used as an Ansatz for the energy distribution $P_s(E; t)$. Both this and the normalized equilibrium distribution are decaying exponentially. It is therefore possible to extract the exponential time dependence from both and write the two distributions as

$$P_s(E; t) = a p_s(E) \mathrm{e}^{-k't}, \quad P_e(E; t) = a p_e(E) \mathrm{e}^{-k't}, \quad (14)$$

where the factor a incorporates the accumulated effect over time of the transient behavior, and hence is not necessarily equal to unity, and p_s, p_e are both normalized to unity (this makes p_e equal to $P_e(E)$ in Eq. (3)). The parameter k', unknown at this point, is the decay constant one measures. Inserting these two populations into Eq. (13) and canceling factors gives

$$-k' p_s(E) = -k(E) p_s(E) - k_e p_s(E) + k_e p_e(E). \quad (15)$$

Integrating over the energy immediately gives

$$k' = \int_0^\infty k(E) p_s(E) \mathrm{d}E. \quad (16)$$

Rearranging Equation (15) gives the energy distribution that is required to calculate this integral:

$$p_s(E) = k_e \frac{p_e(E)}{k(E) + k_e - k'}. \quad (17)$$

Combining Equations (16) and (17) provides an equation for the determination of k';

$$k' = k_e \int_0^\infty \frac{k(E)}{k(E) + k_e - k'} p_e(E) \mathrm{d}E. \quad (18)$$

A somewhat similar expression is given in (Malpathak & Hase, 2019). The differences from this work are that their k_e is identified with a gas collision frequency, which seems an unnecessary assumption, and that k' is absent from the denominator in the integrand.

Equation (18) is the key equation that describes the value of the observed rate constant k' in the steady state exponential decay. The equation generally does not lend itself to easily determined closed form solutions, but some properties can be extracted. The value $k' = k_e$ is a solution to the equation. However, this value leads to both mathematical inconsistent and unphysical distributions. This is seen by introducing this solution into Equation (17) and noting that $k(E)$ is identically zero below the threshold given by the activatio energy. For these energies, $p_s(E)$ becomes infinite over a finite interval.

Another solution exists, as inspection of the left vs. the right hand side of Equation (18) shows, because the curves representing the two sides will in general cross at a value of k' below k_e. We will not go into details of the behavior here, but just point out that considerations of the behavior of these solutions will show that we have the Arrhenius limit $k' \approx k(T)$ for low temperatures and the high temperature limit $k' \approx k_e$. These are also the expected limits, because at high temperatures the bottleneck for decays is not the intrinsic rate constants $k(E)$, but the rate of reheating of the high energy part of the distribution. In other words, in the heating sequence of a molecule M leading to decay, $M(E < E_0) \rightarrow M(E > E_0) \rightarrow M(\text{fragmented})$, where the energy E_0 is defined as $k(E_0) = k'$, the speed of the first reaction is the rate defining. Conversely, at low temperatures the last rate is the defining. The high and low temperature limits are then those for which most of the energy distributions are respectively above or below the energy E_0. In terms of thermally average rate constants $\overline{k}$, the two limits are $\overline{k} \gg k'$ and $\overline{k} \ll k'$.

The model system's numerically calculated distribution p_s distribution for $T = 1500$ K is shown in Figure 4, together with the equilibrium distribution, p_e.

Figure 5 shows the numerical solution of Equation (18) for $k_e = 10^3, 10^6, 10^9$ s^{-1}, for a range of temperatures. It is abundantly clear that the rate constants are strongly influenced by the finite value of the re-equilibration constant already for $k_e = 10^6$ s^{-1}, and even more so for the lower value of k_e, where the measured rate constants can be wrong by an order of magnitude or more, even at temperatures where it is orders of magnitude smaller than the re-equilibration constant.

A note on the value of the re-equilibration constants used here is in place. In a gas with a thermal speed of v, a collision cross section σ, and a density of N/V, the collision frequency is

$$f = \sigma v \frac{N}{V}. \quad (19)$$

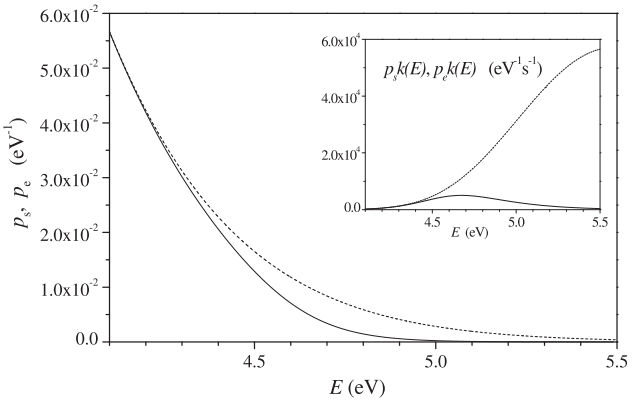

FIGURE 4. The equilibrium energy distribution for the model system of Equation (12) (dashed line), and the modified long time energy distribution p_s (full line) for $k_e = 10^6$ s^{-1}, shown in the energy range where the latter is depleted by decay. The difference between the two is responsible for the difference of more than a factor 20 between the Arrhenius value and the asymptotic curve for the same k_e-value used in Figure 3. The inset shows the product of the rate constants and the two distributions for the same abscissa values, for an illustration of the reason for the large effect that occur out of the small difference between the two distributions.

With a numerical example using a temperature 1500 K, a pressure of one atmosphere, the mass 100 u, the cross section 100 Å^2, and the ideal gas law to calculate the molecular density, the collision frequency f is on the order of $f \sim 2 \times 10^9$ s^{-1}. But for an activated process, this is not the re-equilibration time constant, which is far smaller. The bulk part of the energy distribution is located around the equilibrium mean thermal energy. To move such an energy into the decaying part of the distribution requires a minimum number of collisions, $n_{\min}$, equal to the relevant energy difference divided by the average energy transfer per collision.

For the example with an activation energy of 3 eV, the absolute minimum amount needed to fragment is this threshold energy. Subtracting the thermal energy at the assumed temperature of 1500 K means 2.3 eV needs to be transferred to the molecule by collisions. With an energy transfer of 1500 K, equal to 0.13 eV, per collision, we get an order of magnitude estimate equal to $n_{\min} \sim \frac{2.3\,\text{eV}}{0.13\,\text{eV}} = 17$, where the denominator is the thermal kinetic energy.

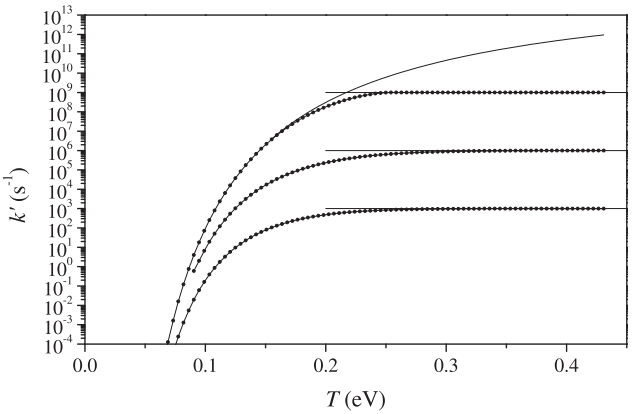

FIGURE 5. The rate constants calculated self-consistently with Equation (18) for the re-equilibration rates $k_e = 10^3$, 10^6, and 10^9 s^{-1} (circles, bottom to top). The full, curved line is the Arrhenius rate constant, and the horizontal lines are the associated values of k_e.

As the energy transfer process is statistical, effectively a random walk, a better estimate of the average number of collisions required to induce decay is given by the square of this number; $\bar{n} \sim n_{\min}^2$. The estimate of the value of k_e for the collision frequency considered is therefore closer to $k_e \sim 6 \times 10^6 \text{s}^{-1}$ than to the more than two orders of magnitude larger collision frequency.

The approximate nature of this estimate should be stressed. A more precise estimate than this would require a more detailed study (see e.g., Smith, 1997; Houston, Conte, & Bowman, 2014; Matsugi, 2018, 2019 for numerical studies).

The conclusions of this simple model is that the re-equilibration constant plays an important role in determining observed decay rates, even in the exponential regime, and that in the absence of any significant re-equilibration mechanism, the exponential decay fails completely and must be replaced by another description.

III. DERIVATION OF THE 1/T DECAY RATE

It is clear from the preceding section that thermal decays will in general not be exponential even if energy distributions are sampled from distributions that are initially canonical. It is also clear that even if a state with exponential decay is eventually reached, the latency time increases with the decrease of the re-equilibration rate. In the limit of no re-equilibration, the transient part of the curve is the only part observed.

The shape of this part of the curve is already suggested in Figure 2. For a general derivation of the shape of the infinitely long transient part of the curve, consider the expression for the decay rate, i.e. the negative derivative of the abundances, I, with respect to time,

$$R = -\frac{\mathrm{d}I}{\mathrm{d}t}, \tag{20}$$

where I is the integrated form of the energy-specified density of internal excitation energy, $g(E; t)$:

$$I \equiv \int_0^\infty g(E; t)\mathrm{d}E. \tag{21}$$

The rate defined in Equation (20) is the one measured in e.g. storage rings. The time-integrated form is measured as the so-called metastable decay fraction in single pass devices such as mass spectrometers. In the absence of re-equilibration the energy-specified abundance can be factorized into an initial distribution, $g(E)$, and a time dependent survival probability, $P_{sur} \leq 1$ as

$$g(E; t) = g(E)P_{sur}(E; t). \tag{22}$$

The salient point of this separation is that the survival fraction P_{sur} depends on energy and that for statistical decays, it can be written as the energy-specified exponential decay:

$$P_{sur}(E) = \exp(-k(E)t). \tag{23}$$

As before, t is the time between the creation of the distribution $g(E)$ in the source and the time of measurement. Using P_{sur}, $g(E; t)$ and I with Equation (20) gives the decay rates

$$R(t) \propto \int_0^\infty g(E)k(E)\exp(-k(E)t)\mathrm{d}E. \tag{24}$$

In the first, simplest description, $g(E)$ can be assumed constant. The integrand of Equation (24) has a maximum emission rate as a function of energy given by

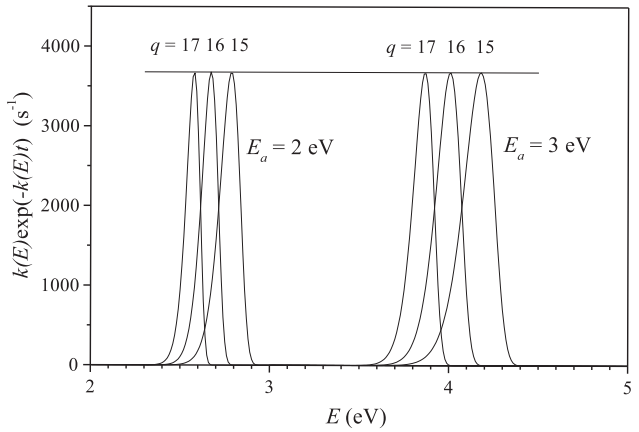

FIGURE 6. The product $k(E)\exp(-kt)$ at $t = 100\,\mu s$ for a rate constant with different frequency factors and different activation energies. Although the peak energies and the widths of the distributions are clearly different, the peak values are seen to be identical and equal to the value $\exp(-1)/t$, which is indicated by the horizontal line.

$$\frac{\mathrm{d}}{\mathrm{d}E}k(E)\exp(-k(E)t) = 0 \Rightarrow k(E)t = 1. \tag{25}$$

Hence the decay rate will have its peak value at $\exp(-1)/t$. It is noteworthy that this result is independent of the expression for k. The only assumption made is that the derivative of k with respect to energy is non-zero. This is valid most of the time, but melting/freezing can invalidate this assumption. See below for an example.

Some examples calculated numerically are shown in Figure 6. The rate constants for the six curves in the figure are calculated with variations of the quasi-realistic expression previously used, which represents variations of the approximate formula for the decay of a harmonic oscillator cluster of nine atoms:

$$k(E) = 10^{q}\mathrm{s}^{-1}\left(\frac{E - E_a}{E}\right)^{3\cdot 9-7}, \tag{26}$$

where q is a parameter which provides a simple parametrization of the rate constant. The figure demonstrates very clearly that the peak values of the rate constants are completely independent of these decay constant parameters.

As it is clear from Equation (23) the nonexponential decays that will be derived below based on that equation do *not* reflect a non-statistical decay of individual clusters. A $g(E)$ which is sufficiently close to a delta function will obviously still reproduce an exponential decay, at least when only a single decay is considered. A chain of sequential decays will not be exponential even if initiated from a single size with a delta function energy distribution.

The result that the energy-specified decay rate peaks at $\exp(-1)/t$ suggests that the total decay rate has a similar time dependence. The total rate can be found by integration over the distributions analogous to the ones shown in Figure 6. As an alternative it will here be calculated with a approximate rate constant to show that a power law appears naturally and that this result does not depend on the rate constants' precise functional forms. This is followed by a more detailed calculation to derive the factors that multiply $1/t$.

In the first step the rate constant is approximated for the relevant and fairly limited energy interval as

$$k(E) = k_0\mathrm{e}^{\alpha(E-E_0)}, \tag{27}$$

where α is a positive but so far unspecified constant. This form is chosen to represent any rate constant that varies sufficiently rapidly with energy. Although a number of different expressions for unimolecular rate constants have been proposed, they all share this rapid variation with energy, and it must be considered a safe parametrization. The relevant energies here are the ones for which $k(E) \sim 1/t$. This translates into a fairly low energy per degree of freedom and a rather steep curve of k versus E. Even for experiments on long time scales will the difference in energy at the start and the experiment therefore be fairly small.

The energy for which the decay rate $k(E)\exp(-k(E)t)$ peaks, E_m, is found by equating Equation (27) to $1/t$ and solving for E:

$$E_m = E_0 - \alpha^{-1}\ln(k_0 t). \tag{28}$$

Crucially, this is also the energy that divides between the systems with energies too low to have decayed and those with too high energy to have survived at time t. The energy is time dependent, and for broad and flat energy distributions the decay rate is therefore proportional to the negative of the rate of decrease of this energy:

$$R(t) \propto -\frac{\mathrm{d}E_m(t)}{\mathrm{d}t} = \alpha^{-1}\frac{1}{t}, \tag{29}$$

where the constant of proportionality left out from the first equality is the density of excitation energies, . The mutually dependent choices of k_0 and E_0 cancel, and the result depends only on α.

Specifying the rate constant to find the value of α, Equation (7) is applied here.

$$k(E) = \omega\left(1 - \frac{E_a}{E}\right)^{s}. \tag{30}$$

To connect to the value of α, the logarithm of Equation (30) is expanded in E. Using the energy given by $k(E) = 1/t$ as the expansion point results in the coefficient

$$\alpha^{-1} = \frac{E_a}{s(1 - (\omega t)^{-1/s})^2}. \tag{31}$$

This makes the decay rate in Equation (29) proportional to E_a, which has a straightforward dimensional interpretation; The decay rate is proportional to the density of excitation energy, $g(E)$, which has dimension of 1/energy. The only other parameter of dimension that appears in the problem is E_a, and consequently the rate must be proportional to $E_a g(E)$.

The dependence on s is less easy to understand in the form it appears in Equation (31). The following expansion will shed some light on the question:

$$\begin{aligned} 1 - (\omega t)^{-1/s} &= 1 - \mathrm{e}^{-\ln(\omega t)/s} \\ &= 1 - (1 - \ln(\omega t)/s + (\ln(\omega t)/s)^2/2 - \cdots) \\ &= \ln(\omega t)/s - (\ln(\omega t)/s)^2/2 + \cdots \end{aligned} \tag{32}$$

As the dependence on frequency and time in this expression is logarithmic, there is fairly little variation in the values of $\ln(\omega t)$, and the range is typically limited to between 20 and 30. This range holds for emission of both electrons (Andersen, Bonderup, & Hansen, 2002) and atoms (Gspann, 1986; Hansen & Campbell, 2004), although the values for electron emission and for systems that are both small and very cold, such as small helium droplets (Brink & Stringari, 1990), tend to be a little

lower. For loss of small fragments with rotational degrees of freedom, the ω increases due to the larger phase space of the products and the logarithm can have values between 35 and 40 (Hansen, Campbell, & Echt, 2006).

For not too small values of s, second term and higher order terms in the expansion can be ignored and the rate therefore expressed as

$$R(t) \propto \frac{sE_a}{\ln(\omega t)^2}\frac{1}{t}. \tag{33}$$

This is identical to the exact result one obtains for a rate constant of the form $k(E) = \omega\exp(-E_a s/E)$, i.e. equivalent to an Arrhenius expression with the emission temperature identified with E/s.

The expression in Equation (33) is derived for a specific and somewhat idealized situation, and it is of interest to have a more general expression. The generalization that will be applied here consists in parametrizing the level densities of both reactant and product as

$$\rho_i(E) = a_i(E + E_i)^{s_i} \tag{34}$$

where subscript $i = r, p$ can denote either reactant (r) or product (p). For the special case of harmonic oscillators, for example, the value of E_i is the zero point energy of the oscillators in the high energy limit. As such it gives the energy offset in the canonical caloric curve $E(T) = (s_i + 1)T - E_i$ for either of the two systems at the relevant temperature range. Similarly, $s_i + 1$ is the canonical heat capacity, and a_i related to the entropy, although the connection is not as simple as that for the two other parameters. The expression covers a lot more ground than just harmonic oscillator systems, although it is still an approximate relation.

The more general expression for a rate constant in Equation (5) then reads

$$k(E) = \omega\frac{a_p(E + E_p - E_a)^{s_p}}{a_r(E + E_r)^{s_r}}. \tag{35}$$

Relating this to the exponential form

$$k(E) \approx \omega' \mathrm{e}^{-\frac{E'_a}{T'}}, \tag{36}$$

requires the calculation of the primed parameters that enter the expression. As pointed out in (Hansen, 2018b) the definition of the temperature and the assignment of a value to the frequency factor are related and they cannot be determined without the application of another criterion. The criterion that was applied in (Hansen, 2018b) was that the caloric curve should be linear;

$$E = C_v T' - E_0. \tag{37}$$

This choice was motivated by the desire to have the simplest possible relation between excitation energy and measurement time. This facilitates the description of decays and it provides directly the interpretation of measurements of metastable decays, for example. It does mean that also C_v and E_0 need to be determined. The somewhat lengthy calculation was reported in (Hansen, 2015) and only the results will be given here. The (re-)defined quantities were found to be the following:

$$\Delta s \equiv (s_r + s_p)/2, \tag{38}$$

$$E'_a \equiv E_a + E_r - E_p, \tag{39}$$

$$(40)\omega' \equiv \omega\frac{a_p}{a_r}[(E + E_r - E'_a)(E + E_r)]^{-\Delta s/2}, \tag{40}$$

$$\bar{s} \equiv \frac{1}{2}(s_r + s_p), \tag{41}$$

$$G \equiv \ln(\omega' t), \tag{42}$$

$$\begin{aligned} E_0 &\equiv E'_a\frac{G}{\bar{s}}\left(1 - \mathrm{e}^{-G/\bar{s}}\right)^{-2} - E'_a\left(1 - \mathrm{e}^{-G/\bar{s}}\right)^{-1} + E_r \\ &\approx -E'_a\left(\frac{1}{2} + \frac{G}{6\bar{s}}\right) + E_r, \end{aligned} \tag{43}$$

$$C_v \equiv \frac{G^2}{\bar{s}}\mathrm{e}^{-G/\bar{s}}\left(1 - \mathrm{e}^{-G/\bar{s}}\right)^{-2}. \tag{44}$$

Two of these results are of special interest. One is that the activation energy of a process (Eq. (39)) is corrected by a value equal to the difference between the energy offsets of the two caloric curves involved. For harmonic oscillators, this corresponds to the difference between the two zero point energies, $\sum_j \hbar\omega_j/2$. For identical average frequencies, $\bar{\omega}$, and a decay by atomic evaporation, this becomes a correction of $E'_a = E_a + 3\hbar\bar{\omega}/2$. The other point is that the effective heat capacity, which has the large cluster behavior $C_v = \bar{s} - G^2/12\bar{s}$, reduces to zero faster than the number of vibrational degrees of freedom when the cluster size is reduced.

In summary, the decay rate is then given by

$$R(t) \propto \frac{C_v E'_a}{\ln(\omega' t)^2}\frac{1}{t}, \tag{45}$$

where the parameters are given in Equations (39), (44), and (40). This expression reproduces the simple interpretation of the rate as the negative of the time derivative of the highest energy in the ensemble:

$$R(t) \propto -\frac{\mathrm{d}E_m}{\mathrm{d}t} = -\frac{\mathrm{d}}{\mathrm{d}t}\frac{C_v E'_a}{\ln(\omega' t)}. \tag{46}$$

In the following we will dispense with the primes, but the reader should keep in mind the physical interpretation of parameters extracted from experimental measurements. Figure 7 shows the results of a series of simulations using Equation (24) with different values of system parameters. The figure includes a case of an energy distribution consisting of a sum of delta functions spaced equidistantly with a 3 eV separation to simulate photon absorption statistics.

A remark on the zero of time are in place. So far it has been assumed to be equal to the production time in a source. This may need to be modified when one observes the products of decay chains of the form $X_N \rightarrow X_{N+1} + X \rightarrow X_{N-2} + 2X \rightarrow \cdots$. Such decay chains are typical for clusters produced in hot sources without forced post-production cooling. For clusters with sufficiently small heat capacities, consecutive decays involve decay constants with widely different values, with all but the last decay happening in a very short time. In those cases, the accumulated time of all decays prior to that of the measured cluster size can be ignored.

This simple approximation changes when consecutive decay constants in a decay chain are not widely different. This occur when heat capacities are sufficiently large. The heat

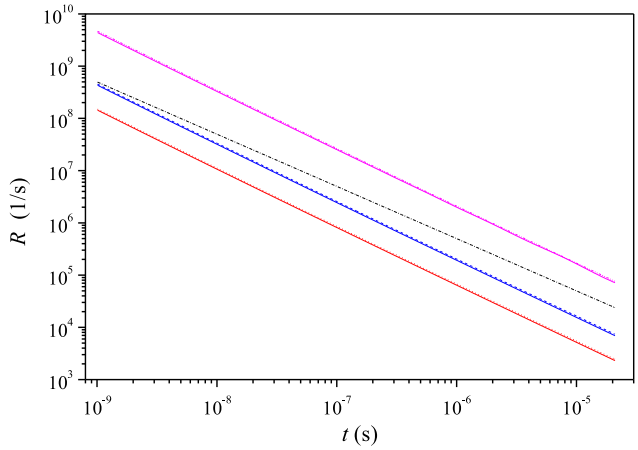

FIGURE 7. Three pairs of simulated decay curves and a single $1/t$ curve (dashed dotted). A pair of simulated curves consists of one curve calculated with a numerical integration of Equation (24) (the solid line in all three cases), and another curve calculated with Equation (45) with the C_v given by Equation (44). The intensities are directly comparable in each pair. The simulated and the calculated curves are almost identical, verifying the quality of the analytical results. From below the parameters are $E_a = 1$ eV, $\bar{s} = 30$, $\omega = 10^{15}$ s^{-1}, $g(E) = 1$/eV (red curves); $E_a = 1$ eV, $\bar{s} = 30$, $\omega = 10^{15}$ s^{-1}, $g(E) = 1$/eV (blue curves); the reference $1/t$ dependence is plotted as a dashed-dotted line (black curve); $E_a = 1$ eV, $\bar{s} = 300$, $\omega = 10^{15}$ s^{-1}, $g(E) = \sum_{n=0}^{\infty} \delta(E - n{\cdot}3\text{eV})$ (magenta curves). The major contribution to the deviation from the $1/t$ is the term $-2/\ln(\omega t)$ (see next section). [Color figure can be viewed at wileyonlinelibrary.com].

capacity where this point is reached is the value (Hansen and Näher, 1999)

$$C_v \approx \ln(\omega t)^2. \tag{47}$$

The size where this value is reached corresponds to clusters of a few hundred atoms for harmonic oscillator heat capacities. For clusters of this and larger heat capacities, the time consumed in the initial decays cannot be ignored. A detailed analysis of the energy distributions produced in ensembles of clusters above such sizes shows that the power law decay appears also for these. This behavior of large clusters is non-trivial and considerations involving energy distributions and any quantity hinging on these distributions require considerations that differ from those used in the main narrative of this work. Details will take us too far astray and the interested reader is referred to (Näher & Hansen, 1994; Hansen & Näher, 1999) for a detailed analysis of the question.

IV. MODIFICATION OF $1/t$ RATES: INTRINSIC, SOURCE PROPERTIES

The derivation of the power law decay is fairly general, and it has been observed in a number of experimental studies, most often at relatively short times (Hansen & Echt, 1997; Hansen et al., 1999; Andersen et al., 2001; Hansen et al., 2001; Andersen et al., 2003a, b; Tomita et al., 2003; Andersen, Heber, & Zajfman, 2004; Fedor et al., 2005; Toker et al., 2007; Sundén et al., 2009; Froese et al., 2011; Lange et al., 2012; Goto et al., 2013; Martin et al., 2013; Najafian et al., 2014; Martin et al., 2015; Breitenfeldt et al., 2016; Hansen et al., 2017b; Ji et al., 2017; Martin et al., 2017; Anderson et al., 2018; Bernard et al., 2019). However, corrections may arise to these results, both in the power of -1 and in the long term behavior, caused by factors both intrinsic and external to the decaying system. Below, the short term behavior will be parametrized by replacing the power -1 by the parameter $-p$ and contributions to p calculated.

In this section the effects of deviations of $g(E)$ from a constant will be treated, together with the effect of the variations of the quantity $\ln(\omega t)$ (or $(\omega t)^{-1/s}$) jointly with the heat capacity. These two effects are perturbations and will be treated separately. In addition, the effect of a melting transition, which represents a very different situation from the rate constants of Equation (35), will be demonstrated with a theoretical case study.

For decays on the microsecond time scales rates change as a rule of thumb by a factor of 20 for each 10% change in excitation energy. Equivalently, the factor $G \equiv \ln(\omega' t)^2$ changes 15% over a time interval of a factor 10. This introduces a small, albeit non-zero time dependence into the denominator in Equation (45). Also the heat capacity which appears in the rate has a time dependence through its dependence on G. The heat capacity in general depends on the temperature, or for the microcanonical ensemble here, on energy. The energy in turn depends on the time, because we are considering the decays from the edge of the energy distribution, and this edge changes with time. To account for these variations, p is calculated by taking the double-logarithmic derivative of the expression

$$R \propto \frac{C_v}{G^2 t}, \tag{48}$$

with respect to t, using the C_v and G from Equations (42) and (44). The resulting value is

$$p = -\frac{\mathrm{d}\ln(R)}{\mathrm{d}\ln(t)} = -1 - \frac{1}{\bar{s}}\left(1 + \frac{2}{\mathrm{e}^{G/\bar{s}} - 1}\right). \tag{49}$$

For systems with large heat capacities, $\bar{s} \gtrsim G$, this reduces to

$$p \approx -1 - \frac{1}{\bar{s}} - \frac{2}{G}. \tag{50}$$

The last term on the right hand side is often the dominant correction and is on the order of 5–10%. It is not a priori given that a double-logarithmic derivative gives a sufficiently constant value to make the calculated corrections to the power -1 meaningful, but a numerical estimate shows that this is indeed the case over a broad time interval. For examples, see Figure 7.

The calculation of this correction to p is facilitated by the results on the heat capacities in Equation (44), but it should be stressed that the result will be arrived at independently of this and does not hinge on any definition of the temperature, as required.

There are a few other possible intrinsic effects that may influence the value of p. One possibility is that vibrational degrees of freedom are frozen in for the parts of the excitation energy distribution that are sampled at long times. This will effectively be a change of $\bar{s}$ with time. A very clear example of this is shown by the measurements of the thermal electron emission from SF_6^- reported in Menk et al. (2014). The electron affinity of the molecule is about 0.5 eV and together with the long measurement time in the experiment, this sets a fairly low value for the energy per degree of freedom. Although the variation of E with time is logarithmically slow, the effect of the decrease with time on the vibrational excitation is boosted because it enters into the determination of the thermal

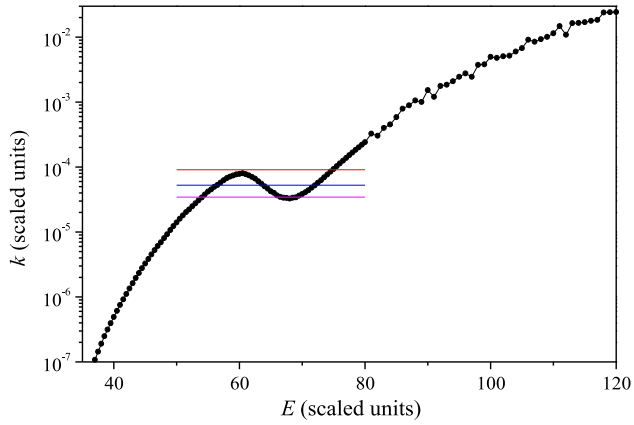

FIGURE 8. The calculated atomic emission rate constant of a cluster of 56 atoms interacting with the Lennard-Jones potential vs. cluster energy. Both energies and rate constants are given in scaled units. The rate constant is calculated by direct simulation of decays for points above $E = 80$. Below that energy, the values are calculated as the detailed balance rate values. The horizontal red, blue and magenta lines, for use with Figure 9, are located at rate constants 1.1×10^4, 1.9×10^4, and 2.7×10^4. [Color figure can be viewed at wileyonlinelibrary.com].

population. The population, in turn, is proportional to what is effectively a Boltzmann factor, $\exp(-\hbar\omega/T)$, which varies very rapidly when the effective temperature T decreases below the vibrational frequency.

Another possible intrinsic effect is that the equivalent of freezing occurs in the particle. The result of a maximum of the rate of $\exp(-1)/t$ also applies to rate constants that are nonmonotonic functions of energy, although the additional peaks that are generated by freezing may not reach the maximum value. Around the melting point at least three more or less resolved peaks will appear in a plot similar to Figure 6.

Figure 8 gives an example of a decay curve that will cause such a behavior. The energy resolved rates are shown in Figure 9 for a range of measurement times that place the energies around the melting point.

The pileup of decays seen in Figure 9 is also seen in the more directly measurable decay rate in the form of an enhanced

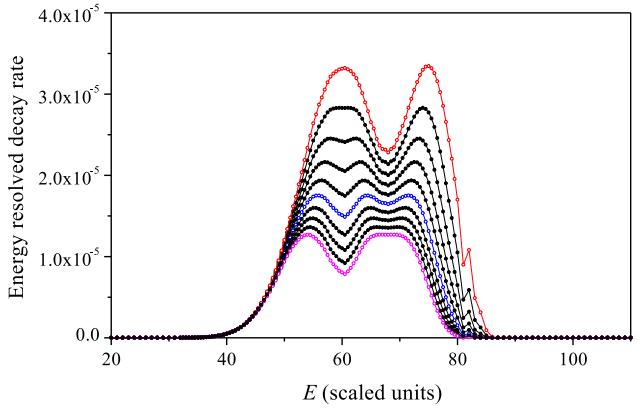

FIGURE 9. The energy resolved decay rate for the cluster with the rate constants shown in Figure 8. The curves are calculated for the scaled times (top to bottom) 1.1×10^4 to 2.9×10^4 in steps of 0.2×10^4. The curves for the times equal to the reciprocal of the three rate constants marked in Figure 8 are rendered in the same colors and the open symbols. [Color figure can be viewed at wileyonlinelibrary.com].

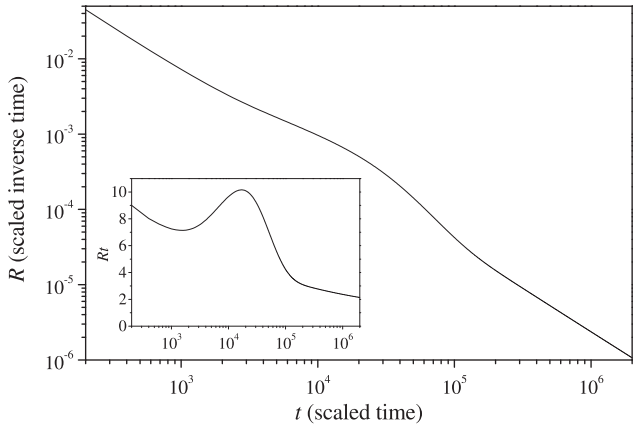

FIGURE 10. The calculated decay rate based on the simulated rate constants shown in Figure 9. The inset shows the product of time and decay rate.

rate at the times where the decays occur from clusters with energies around the freezing point. Figure 10 shows the decay rate for such a situation. Curves such those in Figure 10 have not yet been measured. As seen from the abscissa values, they require that decay rates are measured over a wide range of times. This is feasible with storage rings, in particular of the cryogenic types, where storage times can reach thousands of seconds. In the choice of cluster material due consideration should be paid to effects of radiative cooling (see below).

Finally, the effect of the source should be considered. Even if the excitation energies acquired in a source are sufficient to induce a spontaneous decay, the excitation energy distributions are rarely completely flat. This will affect the measured decay rates. As this is an external input to the problem, it will vary with the type and operating conditions of the source, as well as the particle type. These effects will be included summarily with a single parameter, b, in the description of the energy distribution which is valid over a limited energy interval,

$$g(E) = a\mathrm{e}^{bE}. \tag{51}$$

The value of a is uninteresting in this connection. The decay rate will be given by Equation (46) multiplied by the additional factor $g(E)$. The double-logarithmic derivative gives for the power

$$p \to p + b\frac{E_a C_v}{\ln(\omega t)^2}. \tag{52}$$

The value of b is not observed directly, as a rule. However, if one observes the abundances produced by a cascade of decays of a collection of clusters of different sizes, the energy distributions represented by b can be related to the abundances (see Hansen, 2018b). Ignoring size-to-size variations in E_a's, the modification of p for the size N_0 is calculated by dividing by E_a and using the parameter b' found from fitting the abundances with the function

$$I_N = a\mathrm{e}^{b'(N-N_0)}. \tag{53}$$

Size-to-size variations in I_N should be ignored in the fits of this kind, and only the smooth part of I_N vs. N should be used for this purpose.

The result is then

$$p \to p - b' \frac{C_v}{\ln(\omega t)^2}. \tag{54}$$

Usually this is not a numerically important correction.

V. COMPETING CHANNELS

The power law decay finds its most important use when decays are observed to deviate significantly from the $1/t$ form. A condition for the power law to occur with the powers calculated so far is that the observed channel represents the main decay. Any major amount of decay through a parallel dark channel will cause modifications, to the point of converting the decay into a different functional form. Any significant deviation from $1/t$, viz. one that cannot be assigned to an nonconstant energy distribution or a similar minor effect, can therefore often be taken as indication of the presence of a competing channel.

The most important type of such a dark channel is, somewhat paradoxically, the emission of thermal photons. Emission of thermal photons is an important channel in the decays of molecules and clusters at long times, and the process is attracting increasing attention as an essential part of the description of decays in storage rings and similar devices (Møller, 1997; Dahan et al., 1998; Jinno et al., 2004; Bernard et al., 2008; Pedersen et al., 2015), where cryogenic techniques are pushing storage times into the thousands of seconds regime (Lange et al., 2010; Reinhed et al., 2010; Schmidt et al., 2013; Nakano et al., 2017). It should be stressed that although power law decays appear in their most insistent form in these types of devices, there is no reason to suspect that they are not present in, for example, single pass devices (Hansen & Campbell, 1996), although the available dynamic time range in these instruments often renders the specific time dependence difficult to disentangle experimentally from a standard exponential decay.

The division of time scales into an early unimolecular regime and a later radiative one is caused by the difference in decay parameters for these two classes of decays. Unimolecular decays have a frequency factor multiplying the ratio of level densities which is essentially given as

$$\omega = \frac{8\pi\sigma T^2 m}{h^3}, \tag{55}$$

where σ is the attachment cross section for the inverse process, T the microcanonical temperature of the product particle/molecule, m the mass of the small fragment lost, and h Planck's constant. With sticking coefficients around unity, corresponding to geometric cross sections, calculated frequency factors for atomic cluster are in good agreement with those derived from vapor pressure data of the corresponding bulk matter. Figure 11 shows the comparison for a number of metallic elements for which the vapor is predominantly composed of monomers. These values are higher by about two orders of magnitude than the Debye frequencies (also shown) which is often used in heuristic theories.

Equation (55) is derived from detailed balance considerations. This also provides a frequency factor for the thermal electron emission rate constant. The frequency factor is smaller for electron emission due to the much smaller mass of the emitted particle, although it is often boosted by the larger capture cross section and occasionally by the higher temperature at which electron emission tends to be emitted, and it will still be larger than the photon emission value.

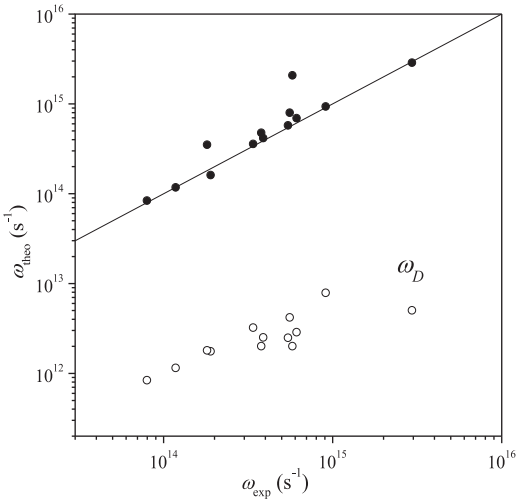

FIGURE 11. The comparison of frequency factors, calculated and extrapolated from bulk vapor pressure, both at the same typical temperatures (closed circles). The values are for surface areas corresponding to a single atom. To get the value for a larger particle, multiply by $N^{2/3}$ or by $(N-1)^{1/3}+1)^2$, which often gives a little better precision. Also shown are the Debye frequencies (open circles).

The parameters of thermal radiation differ from those two types of unimolecular decays in two respects. First of all the activation energy is much smaller. The activation energy is the energy of the lowest optically active excitation in the system. A low energy of this state is necessary for the process to be observed because also the frequency factor for photon emission is smaller than the atomic emission ω's, which is the second difference. The frequency factor is the Einstein A-coefficient, which takes values on the order of 10^9 s^{-1} for typical electronic transitions, but with a significant spread in values. In a canonical situation the photon emission rate constant k_{ph} is, in terms of A and the thermal population of the emitting state, equal to the well-known result

$$k_{ph}(T) = A \frac{e^{-h\nu/T}}{1 - e^{-h\nu/T}}. \tag{56}$$

In a microcanonical situation, this is modified to Andersen, Bonderup, & Hansen (2002)

$$k_{ph}(E) = A \frac{\frac{\rho(E-h\nu)}{\rho(E)}}{1 - \frac{\rho(E-2h\nu)}{\rho(E-h\nu)}}. \tag{57}$$

(At negative energies, level densities are zero.)

With the lower values of both the frequency factor and the activation energy, radiative cooling is bound to dominate the decays at late times and cause a suppression of the unimolecular decay in that time region (Andersen et al., 1996). The details of the description of this suppression depend on the magnitude of the emitted photons. The systematics of this behavior is summarized in a recent review article (Ferrari et al., 2019), and only a few points concerning the influence of thermal radiation on decay rates will be taken up here.

For sufficiently small photon energies, emission of a single photon is insufficient to cause a major change in the unimolecular rate constant. In the other limit a single photon emitted will quench any further decay. Here only the small photon energy limit will be discussed. The large photon limit is treated in (Ferrari et al., 2019).

In the small photon energy limit, the radiative cooling can be considered a continuous process. We can then rewrite Equation (24) by introducing a time dependence due to the radiation, in addition to the time dependence on the exponential depletion. This can in principle be done either by including time dependence in the population, $g(E) \rightarrow g(E,t)$ or in the rate constants, $k(E) \rightarrow k(E,t)$. The latter approach will be used here. With a leading order expansion of the logarithm of the rate constant in the time since creation, one has

$$k(E,t) = k(E,0)\mathrm{e}^{-t/\tau}, \tag{58}$$

where E is the energy the particle is created with, and τ is a time constant, defined as

$$\tau^{-1} = \frac{\mathrm{d}\ln k}{\mathrm{d}E} P_{em}, \tag{59}$$

where P_{em} is the emitted power. The expansion of the logarithm of k and not of k itself is reasonable because of the strong dependence of k on energy and its intrinsic non-negative values.

In terms of the average photon energy $h\overline{\nu}$, and the photon emission constant k_p, the power is

$$P_{em} = h\overline{\nu}k_p. \tag{60}$$

If we stay with the parametrization in terms of a constant value of τ, Equation (24) becomes

$$R(t) \propto \int_0^\infty g(E)k(E)\mathrm{e}^{-t/\tau}\mathrm{e}^{-k(E)\int_0^t \mathrm{e}^{-t'/\tau}\mathrm{d}t'}\mathrm{d}E, \tag{61}$$

where the exponential of the integral gives the surviving fraction at the initial excitation energy E. All time dependence is given explicitly, and the integral is easily calculated to give

$$\begin{aligned} R(t) &\propto \int_0^\infty g(E)k(E)\mathrm{e}^{-t/\tau}\mathrm{e}^{-k(E)\tau(1-\mathrm{e}^{-t/\tau})}\mathrm{d}E \\ &= \mathrm{e}^{-t/\tau}\int_0^\infty g(E)k(E)\mathrm{e}^{-k(E)\tau(1-\mathrm{e}^{-t/\tau})}\mathrm{d}E. \end{aligned} \tag{62}$$

The last equality shows that $\tau(1-\mathrm{e}^{-t/\tau})$ acts as an effective time in the integral, which can then be evaluated simply by copying the previous, nonradiative result with the proper substitution for the time. Including the pre-integral exponential, this converts the power law decay to a quasi-exponential form;

$$R \propto \frac{1}{\tau}\frac{1}{\mathrm{e}^{t/\tau}-1}. \tag{63}$$

The analogous expression for larger photon energies is (stated without proof),

$$R \propto \frac{\mathrm{e}^{-k_p t}}{t}. \tag{64}$$

The expression in Equation (63) reduces to a t^{-1} dependence for short times, as required on physical grounds. At long times it can be approximated by an exponential decay.

The nature of this exponential decay is different from a standard type exponential decay, though, because here the exponential decrease describes the time dependence of the rate constant and not of the population. In fact, at long times, all decays will have ceased but an amount of particles will have been fossilized by the radiation. This is readily observed in storage rings, for example, if the particles are reheated with a laser and resume their decays (Hansen et al., 2001; Kono et al., 2018).

Emission of massive particles may also constitute dark channels. As for photon emission, it will influence the decay rate if it is the main channel, i.e. if the rate constant for this channel is the highest of the two (or more) competing channels on the measurement time scale. One such case is realized in the decay of neutral C_{60} through the channels (Hansen & Echt, 1997)

$$C_{60} \rightarrow C_{60}^+ + e^- \tag{65}$$

$$C_{60} \rightarrow C_{58} + C_2, \tag{66}$$

where only the time-resolved electron yield of the first channel is detected. With k_e, k_a the electron and the C_2 emission rate constant, respectively, the measured electron emission rate is then given by

$$R \propto \int_0^\infty k_e \mathrm{e}^{-(k_e+k_a)t}\mathrm{d}E. \tag{67}$$

Experimentally, the decays were produced by laser excitation and the laser power was varied to ensure that $g(E)$ was flat. It can therefore be left out from the considerations. If the electron yield is dominant, the presence of k_a in the exponential can be ignored, and one then gets a standard power law decay. This is not what is observed. The electron rate varies as

$$R \propto t^{-0.65}. \tag{68}$$

The reduction of the absolute value of the power from unity can only be understood as a consequence of the fact that the C_2 loss channel is dominant. We can therefore write the rate as

$$R \propto \int_0^\infty k_e \mathrm{e}^{-k_a t}\mathrm{d}E. \tag{69}$$

Expressing k_e in terms of k_a using exponential expressions for both with a few simplifications, gives that

$$k_e \propto k_a^{\mathrm{IE}/E_a}, \tag{70}$$

where IE is the ionization energy measured to be 7.6 eV, and E_a is the C_2 loss activation energy. This gives a power law decay

$$R \propto t^{-\mathrm{IE}/E_a}. \tag{71}$$

Although the ionization energy was well known at the time these experiments were performed, the C_2 dissociation energy was not. The measured power in this decay allowed a determination of the value, which was in much better agreement with the values produced in the fairly intensive work with quantum chemical calculations that followed the discovery of the Krätschmer-Huffman method of production of macroscopic amounts of the molecules. The value extracted was around 11 eV. With a few later adjustments to 10.8 ± 0.3 eV (Tomita et al., 2003), this is now the generally accepted value.

VI. ACTION SPECTROSCOPY

Molecules, in particlular large molecules, are occasionally, and clusters very often, found in so low concentrations that standard absorption spectroscopy is not feasible. Although techniques

such as cavity ring-down spectroscopy will be able to render absorption spectroscopy feasible in some situations, a more convenient spectroscopic technique in cluster studies is action spectroscopy. The principle of this method is to use the easily measured loss of a part of a cluster, typically an atom, as a signature for the absorption of one or more photons.

The use of this technique is widespread. For examples on molecular ions, see Dunbar & Fu (1973), Drzaig & Brauman (1984), Wetzel & Brauman (1987), Dunbar (1988), Willey et al., (1991); for clusters, see Borggreen et al. (1993), Collings et al. (1994), Hansen et al. (1999), Vogel, Herlert, & Schweikhard (2003), Gilb et al. (2004), Kaydashev et al. (2016); and for biomolecular ions, see Nielsen et al. (2001), Andersen et al. (2005), Antoine & Dugourd (2013), Yao & Jockusch (2013), Bellina et al. (2014), Harvey et al. (2015), Wellman & Jockusch (2015), Xu et al. (2015), Milne et al. (2016), O'Connor et al. (2017), Woodhouse et al. (2017).

The application of the technique requires that the quantum yield of the decay process is not too low, and if absolute cross sections are desired it should be known. When the action proceeds via a thermal decay, the quantum yield clearly depends critically on the photon energy. The situation is particularly critical at the red end of a spectrum, where photon energies can be too low to induce the signature decay, and for which a vanishing quantum yield can erroneously be interpreted as a vanishing absorption cross section. Although this problem of insufficient heating can to some extent be bypassed with the use of the messenger molecule technique (see below), it is still particularly severe for vibrational spectroscopy, for which multi-photon absorption is required to provide any yield at all, and techniques have been developed for these experimental conditions, taking into account factors such as the variation of the cross section with internal energy etc. (von Helden, van Heijnsbergen, & Meijer, 2003; Bakker et al., 2010). The problem is most severe and also simplest to examine for one photon processes, and in the following only this situation will be considered.

The problem can be quantified and solved when the internal excitation energy distributions are those that give rise to power law decays. Experimentally, the assumption of a broad energy distribution can be tested by measuring the spontaneously appearing decay fraction and comparing with the results given above. To summarize previous equations, the fractional amount of decay of a mass-selected particle should be given approximately by

$$M \equiv \frac{I_d}{I_n + I_d} = \frac{C_v}{(\ln \omega t)^2} \ln\left(\frac{t_2}{t_1}\right), \tag{72}$$

when the integrated yield between t_1 and t_2 is measured. The intensities I_n and I_d denote the number of non-decayed and decayed particles, respectively. If these measurements conform to the calculated yields, the decay can safely be described as statistical and from the broad energy distributions assumed here.

The problem of calculating the yield involves several different experimental times, viz. the time between production and measurement, the time lag between photon absorption and the start of the recording of the decay, which may be but not necessarily is zero, and the time where the measurement of the metastable decay ends. If present, radiative cooling will also have to be included in the analysis. We will assume here that radiative cooling is not present. The case where it is present has been treated in (Hansen, 2018a), to which the interested reader is referred.

In a spectroscopy experiment, the cross section, σ, is obtained from the photo-induced decay count rate I as

$$\sigma \propto \frac{I}{\Phi F}, \tag{73}$$

where F is the photon flux and Φ is the quantum yield, defined as the number of reactions per absorbed photon. For a thermally induced decay, by nature a delayed reaction, the quantum yield depends on the measurement time, the photon energy, and also on the internal energy. Denoting the differential (energy-specified) quantum yield by ϕ, we can write

$$\phi = \phi(E, h\nu, t_1, t_2), \tag{74}$$

where t_1, t_2 are the beginning and the end of the experimental detection window, i.e. the limits of the time interval during which the decay is measured. The total yield is an integral over the energy dependent contributions from the different excitation energies:

$$\Phi(h\nu, t_1, t_2) = \int \phi(E, h\nu, t_1, t_2) g(E - h\nu) \mathrm{d}E, \tag{75}$$

where $g(E)$ is the distribution of excitation energies immediately before the photon absorption that happens at time t_{las}. As before, the zero of time is conveniently set to the time of creation in the source. Setting g to unity, the quantum yield becomes, after taking depletion up to t_{las} into account,

$$\Phi(h\nu, t_1, t_2) = \int \phi(E, h\nu, t_1, t_2) \mathrm{e}^{-k(E-h\nu)t_{las}} \mathrm{d}E. \tag{76}$$

The fraction σF of the energy distribution is shifted up by the photon energy $h\nu$ upon absorption. The energy distribution becomes

$$P(t_{las}, E) = \mathrm{e}^{-k(E)t_{las}}(1 - \sigma F) + \sigma F \mathrm{e}^{-k(E-h\nu)t_{las}}. \tag{77}$$

This distribution has the time development

$$P(t, E) = P(t_{las}, E)\mathrm{e}^{-k(E)(t-t_{las})} = \mathrm{e}^{-k(E)t}(1 - \sigma F) + \sigma F \mathrm{e}^{-k(E-h\nu)t_{las} - k(E)(t-t_{las})}. \tag{78}$$

To find the change in population due to photon absorption at the high energy side, which is the relevant one for the question at hand, subtract the non-photo-excited population;

$$P_p(t, E) \equiv P(t, E) - P_0(t, E) = \sigma F(\mathrm{e}^{-k(E-h\nu)t_{las} - k(E)(t-t_{las})} - \mathrm{e}^{-k(E)t}). \tag{79}$$

This is non-negative anywhere and as the time derivative of it is negative, the differences calculated below for the yields are all non-negative as required, although this may not be immediately apparent from the expression. The energy-specified quantum yield for a photon-enhanced decay is the difference between the populations in Equation (79) at t_1 and t_2:

$$\begin{aligned}\phi(E, h\nu, t_1, t_2) &= P_p(t_1, E) - P_p(t_2, E) \\ &= \mathrm{e}^{-k(E-h\nu)t_{las} - k(E)(t_1 - t_{las})} - \mathrm{e}^{-k(E)t_1} \\ &\quad -\mathrm{e}^{-k(E-h\nu)t_{las} - k(E)(t_2 - t_{las})} + \mathrm{e}^{-k(E)t_2}\end{aligned} \tag{80}$$

The total quantum yield follows from integrating over all energies:

$$\Phi = \int_0^\infty [\mathrm{e}^{-k(E-h\nu)t_{las}-k(E)(t_1-t_{las})} - \mathrm{e}^{-k(E)t_1} - \mathrm{e}^{-k(E-h\nu)t_{las}-k(E)(t_2-t_{las})} + \mathrm{e}^{-k(E)t_2}]\mathrm{d}E. \quad (81)$$

All times entering Equation (81) are instrumental and the quantum yield can be calculated if the functional form for the rate constant is known.

It is possible to reduce the number of parameters needed to calculate the yield. Define the fictitous time t_0 as

$$k(E - h\nu)t_{las} \equiv k(E)t_0. \quad (82)$$

It is clear from the definition that t_0 is positive. It does not depend on the frequency factor that appears in the description of the rate constant (it appears on both sides of the equation as a multiplicative factor and cancels). The value of t_0 can therefore be calculated from level densities and activation energies alone. Although t_0 is introduced as a fictitious time, it has a measurable physical meaning as the zero of time for the photo-excited part of the ensemble. If the time-resolved decay after laser excitation is measured, it is found as the offset in the photo-induced decay as $1/(t - t_{las} + t_0)$. This is particularly easy to measure in storage ring experiments, see e.g. (Sundén et al., 2009), but it is not unique to such experiments; also single pass experiments may accomplish this. The identification of t_0 with the experimental time offset is derived below after some simplifications of the equations.

With the parametrization of the rate constant in Equation (82) for the shifted energy, the signal becomes

$$\Phi \propto \int_0^\infty \mathrm{e}^{-k(E)(t_1-t_{las}+t_0)} - \mathrm{e}^{-k(E)(t_2-t_{las}+t_0)} + \mathrm{e}^{-k(E)t_2} - \mathrm{e}^{-k(E)t_1}\mathrm{d}E. \quad (83)$$

All four terms in the exponent in the integrand of Eq. (83) contain the factor $k(E)$, but are multiplied by different times. As argued, the arguments of the exponentials are strongly varying functions of energy, providing fairly sharp cutoffs in the energy distribution. The cutoff energies, E_m, for the energy distribution for the laser excited species are

$$E_m(t) = \frac{E_a C_v}{\ln(\omega t)} + E_0, \quad (84)$$

where t may be either of the times t_1, t_2, $t_1 - t_{las} + t_0$, $t_2 - t_{las} + t_0$ in Equation (83).

The presence of such a cutoff energy greatly facilitates the calculation of the integral, because these can be calculated as the pairwise differences between the two cutoff energies. The energy offset E_0 cancels in the process and the integral is approximately proportional to

$$\Phi \propto \frac{1}{\ln\omega(t_1 - t_{las} + t_0)} - \frac{1}{\ln\omega(t_2 - t_{las} + t_0)} + \frac{1}{\ln\omega t_2} - \frac{1}{\ln\omega t_1}. \quad (85)$$

The factor $E_a C_v$ is independent of the photon energy and has been left out. The contribution of the last two terms can be approximated by an expansion to first order in $\ln(t_2/t_1)$. This gives the (unnormalized) quantum yield;

$$\Phi \propto \frac{1}{\ln\omega(t_1 - t_{las} + t_0)} - \frac{1}{\ln\omega(t_2 - t_{las} + t_0)} - \frac{\ln t_2/t_1}{(\ln\omega t_{las})^2}. \quad (86)$$

The value of t_0 can be calculated if some information about the energy dependence of the decay constant is available. Alternatively, it is possible, as mentioned above, to relate t_0 to the experimentally observable decay rate after the photon absorption. The photon-enhanced decay rate is the derivative of Φ with respect to t_1:

$$R = \frac{\mathrm{d}\Phi}{\mathrm{d}t} \propto \frac{1}{(\ln\omega t_0)^2}\frac{1}{t - t_{las} + t_0} - \frac{1}{(\ln\omega t_{las})^2}\frac{1}{t} \approx \frac{1}{(\ln\omega t_0)^2}\frac{1}{t - t_{las} + t_0}. \quad (87)$$

A fit of the measured R versus $t - t_{las}$ will give t_0 directly. It may be more convenient to fit R^{-1},

$$R^{-1} \propto t - t_{las} + t_0. \quad (88)$$

The derivation here provides the quantum yield for thermal, photo-induced decays from an ensemble of clusters with broad energy distributions, and can be applied directly to convert yields to relative cross sections for these situations. It works also when the messenger atom technique is used, in which a weakly bound atom is detached at a lower energy than the threshold for unimolecular reaction of the undressed cluster. See, e.g., Cismesia et al. (2017) and Gorlova et al. (2017) for two recent examples of work using this technique. The benefit of the messenger atom technique is that it extends the sensitivity of the spectroscopy to a photon energy smaller than the naked cluster technique by a factor $E_{a,atom}/E_{a,naked}$. However, the low internal energies required for an efficient sticking of a messenger atom may be incompatible with the requirement of a broad cluster excitation energy distribution. This is patly an experimental issue which is best addressed for the specific experiment undertaken.

It should also be mentioned that the results can be used when the decaying systems radiate, with the proper modifications of the equations. A detailed analysis of these cases is given in Hansen (2018a).

The main result presented here is an equation for the quantum yield for a given photon energy in an ensemble possessing a broad energy distribution. In this situation the action yields need to be corrected with the quantum yields to give the correct absorption cross section. This is achieved by division with the expression in Equations (86) or (85). The procedure for the nonradiative cases described here involve the determination of the frequency factor of the measured process.

This will usually be by theoretical means, but as it enters only logarithmically, the uncertainty associated with this will have a minor effect. All times except t_0 that enter the expression are experimental values. The value of t_0 is either measured as described, or it is calculated with Equation (82).

VII. CONCLUSIONS AND OUTLOOK

Decays of free particles, without contact with a thermalizing heat bath, will often occur with a power law time dependence,

in spite of being completely statistical and exponential at the level of individual particles. A power law decay does not contain any characteristic time and consequently also no characteristic energy that can be related to the activation energy of the process. It does, however, have a zero of time, in contrast to exponential decays.

The systematics associated with the power law decay has consequences for a number of phenomena. One is the amount of metastable decays, another the relation of hot cluster beam abundances to binding energies. It also has importance when it breaks down. The presence of a competing channel is one such situation. Such a channel will, if dominant, cause distortions of the decay which can be used to identify the characteristics of this dark decay. Frequently observed cases involve thermal photon emission.

The technique of using deviations from power law decays to infer the properties of a dark competing channel has been used for the decay spectra of metal cluster anions in some of the presently longest storage time experiments at electrostatic ion storage rings (Hansen et al., 2017b; Anderson et al., 2018). In these experiments, made possible by the low device temperatures which reduce the pressure and hence the limiting factor of restgas collisions, the ions can be stored for a good fraction of an hour. This permits the identification of more than one radiatively suppressed power law decay in the decay of an ionic species. Small copper clusters, for example, have been observed to decay with two such curves (Breitenfeldt et al., 2016; Hansen et al., 2017b). They have been identified as originating from two different populations of the cluster ions, differing by their angular momenta (Hansen et al., 2017b). This conserved quantity acts as a very efficient barrier, blocking the conversion between the two types of isomers and endowing them with different radiative properties, making their observation possible by simple measurements of the decay rates.

In summary, the power law decay of isolated and highly excited ions is both well established and useful for the interpretation of a number of phenomena. It appears in its most insisting form in long term storage devices, but is often present in single pass devices also, even if much harder to distinguish from the more commonly used fitting functions of exponential decays.

REFERENCES

Andersen J, Cederquist H, Forster J, Huber B, Hvelplund P, Jensen J, Liu B, Manil B, Maunoury L, Brøndsted Nielsen S, Pedersen U, Schmidt H, Tomita S, Zettergren H. 2003a. Power-law decay of collisionally excited amino acids and quenching by radiative cooling. Eur Phys J D 25:139–148.

Andersen J, Gottrup C, Hansen K, Hvelplund P, Larsson M. 2001. Radiative cooling of fullerene anions in a storage ring. Eur Phys J D 17(2):189–204.

Andersen JU, Bonderup E, Hansen K. 2002. Thermionic emission from clusters. J Phys B At Mol Opt Phys 35:R1.

Andersen JU, Bonderup E, Hansen K, Hvelplund P, Liu B, Pedersen U, Tomita S. 2003b. Temperature concepts for small, isolated systems; 1/*t* decay and radiative cooling. Eur Phys J D 24:191–196.

Andersen JU, Brink C, Hvelplund P, Larsson MO, Nielsen BB, Shen H. 1996. Radiative cooling of C_{60}. Phys Rev Lett 77:3991–3994.

Andersen LH, Heber O, Zajfman D. 2004. Physics with electrostatic rings and traps. J Phys B: At Mol Opt 37:57–88.

Andersen LH, Nielsen IB, Kristensen MB, ElGhazaly MOA, Haacke S, Nielsen MB, Petersen MA. 2005. Absorption of Schiff-base retinal chromophores in vacuo. J Am Chem Soc 127:12347–12350.

Anderson EK, Kamińska M, Chartkunchand KC, Eklund G, Gatchell M, Hansen K, Zettergren H, Cederquist H, Schmidt HT. 2018. Decays of excited silver cluster anions Ag_n^-, $n = 4$ to 7 in the Double ElectroStatic Ion Ring ExpEriment. Phys Rev A 98:022705.

Antoine R, Dugourd P. 2013. Photophysics of ionic biochromophores. In: SB Nielsen, J Wyer, editors, Physical chemistry in action, chapter UV-visible absorption spectroscopy of protein ions, pp. 141–153. Berlin, Heidelberg: Springer.

Arrhenius S. 1889. Über die Reaktionsgeschwindigkeit bei der Inversion von Rohrzucker durch Säuren. Z physik Chem 4:226.

Bakker JM, Lapoutre VJF, Redlich B, Oomens J, Sartakov BG, Fielicke A, von Helden G, Meijer G, van der Meer AFG. 2010. Intensity-resolved IR multiple photon ionization and fragmentation of C_{60}. J Chem Phys 132:074305.

Bellina B, Brown JM, Ujma J, Murray P, Giles K, Morris M, Compagnon I, Barran PE. 2014. UV photodissociation of trapped ions following ion mobility separation in a Q-ToF mass spectrometer. Analyst 139:6348–6351.

Bernard J, Al-Mogeeth A, Allouche A-R, Chen L, Montagne G, Martin S. 2019. Photo-dissociation of naphthalene dimer cations stored in a compact electrostatic ion storage ring. J Chem Phys 150:054303.

Bernard J, Montagne G, Brédy R, Terpend-Ordacière B, Bourgey A, Kerleroux M, Chen L, Schmidt HT, Cederquist H, Martin S. 2008. A "tabletop" electrostatic ion storage ring: Mini-ring. Rev Sci Instrum 79(7):075109.

Borggreen J, Chowdhury P, Kebaïli N, Lundsberg-Nielsen L, Lützenkirchen K, Nielsen MB, Pedersen J, Rasmussen HD. 1993. Plasma excitations in charged sodium clusters. Phys Rev B 48:17507.

Breitenfeldt C, Blaum K, Froese MW, George S, Guzmán-Ramírez G, Lange M, Menk S, Schweikhard L, Wolf A. 2016. Decay processes and radiative cooling of small anionic copper clusters. Phys Rev A 94:033407.

Brink DM, Stringari S. 1990. Density of states and evaporation rate of helium clusters. Z Phys D 15:257–263.

Cismesia AP, Tesler LF, Bell MR, Bailey LS, Polfer NC. 2017. Infrared ion spectroscopy inside a mass-selective cryogenic 2D linear ion trap. J Mass Spectrom. 52:720–727.

Collings BA, Athanassenas K, Lacombe D, Rayner DM, Hackett PA. 1994. Optical absorption spectra of Au_7, Au_9, Au_{11}, and Au_{13}, and their cations: Gold clusters with 6, 7, 8, 9, 10, 11, 12, and 13 s-electrons. J Chem Phys 101(5):3506–3513.

Dahan M, Fishman R, Heber O, Rappaport M, Altstein N, Zajfman D, van der Zande WJ. 1998. A new type of electrostatic ion trap for storage of fast ion beams. Rev Sci Instrum 69:76.

Drzaig PS, Brauman JI. 1984. A determination of the triplet singlet splitting in phenylnitrene via photodetachment spectroscopy. J Am Chem Soc 106:3443–3446.

Dunbar RC. 1988. Laser photodissociation techniques for studying ion spectroscopy and structure. Anal Instrum 17:113–130.

Dunbar RC. 2004. BIRD (blackbody infrared radiative dissociation). Mass Spectrom Rev 23:127–158.

Dunbar RC, Fu EW. 1973. Photodissociation spectroscopy of gaseous $C_7H_8^+$ cations. J Am Chem Soc 95:2716–2718.

Echt O, Sattler K, Recknagel E. 1981. Magic numbers for sphere packings: experimental verification in free xenon clusters. Phys Rev Lett 47:1121.

Fedor J, Hansen K, Andersen JU, Hvelplund P. 2005. Nonthermal power law decay of metal dimer anions. Phys Rev Lett 94:113201.

Ferrari P, Hansen K, Lievens P, Janssens E. 2018a. Stability of small cationic platinum clusters. Phys Chem Chem Phys 20:29085–29090.

Ferrari P, Janssens E, Lievens P, Hansen K. 2015. Thermal radiation and fragmentation pathways of photo-excited silicon clusters. J Chem Phys 143:224313.

Ferrari P, Janssens E, Lievens P, Hansen K. 2019. Radiative cooling of size-selected gas phase clusters. Int Rev Phys Chem 38:405–440.

Ferrari P, Vanbuel J, Hansen K, Lievens P, Janssens E, Fielicke A. 2018b. Effect of radiative cooling on the size-dependent stability of small boron clusters. Phys Rev A 98:012501.

Froese MW, Blaum K, Fellenberger F, Grieser M, Lange M, Laux F, Menk S, Orlov DA, Repnow R, Sieber T, Toker Y, vonHahn R, Wolf A. 2011. Thermionic power-law decay of excited aluminum-cluster anions and its dependence on storage-device temperature. Phys Rev A 83:023202.

Gilb S, Jacobsen K, Schooss D, Furche F, Ahlrichs R, Kappes MM. 2004. Electronic photodissociation spectroscopy of $Au_n^-\cdot$ Xe (n = 7-11) versus timedependent density functional theory prediction. J Chem Phys 121:4619.

Gorlova O, Colvin SM, Brathwaite A, Menges FS, Craig SM, Miller SJ, Johnson MA. 2017. Identification and partial structural characterization of mass isolated valsartan and its metabolite with messenger tagging vibrational spectroscopy. J Am Soc Mass Spectrom 28:2414–2422.

Goto M, Sundén A, Shiromaru H, Matsumoto J, Tanuma H, Azuma T, Hansen K. 2013. Direct observation of internal energy distributions of C_5^-. J Chem Phys 139:054306.

Gspann J. 1986. On the phase of metal clusters. Z Phys D 143–145.

Hansen K. 2015. The effective temperature in microcanonical rate constants. Chem Phys Lett 620:43–45.

Hansen K. 2018a. Action spectroscopy of highly excited molecular ions in molecular beams. Int J Mass Spectrom 430:14–21.

Hansen K. 2018b. Statistical physics of nanoparticles in the gas phase, Volume 73 of *Springer Series on atomic, optical, and plasma physics*. Dordrecht: Springer.

Hansen K, Andersen JU, Cederquist H, Gottrup C, Hvelplund P, Larsson MO, Petrunin VV, Schmidt HT. 1999. Thermionic emission laser spectroscopy of stored C_{60}^-. Eur Phys J D 9:351.

Hansen K, Andersen JU, Hvelplund P, Møller S, Pedersen U, Petrunin V. 2001. Observation of a 1/*t* decay law for hot clusters and molecules in a storage ring. Phys Rev Lett 87:123401.

Hansen K, Campbell E. 2004. Do we know the value of the Gspann parameter? Int J Mass Spectrom 233:215–221.

Hansen K, Campbell EEB. 1996. Radiative cooling of fullerenes. J Chem Phys 104(13):5012–5018.

Hansen K, Campbell EEB, Echt O. 2006. The frequency factor in statistical fullerene decay. Int J Mass Spec 252:79.

Hansen K, Echt O. 1997. Thermionic emission and fragmentation of C_{60}. Phys Rev Lett 78:2337.

Hansen K, Ferrari P, Janssens E, Lievens P. 2017a. Thermal radiation of gold clusters on microsecond time scales. Phys Rev A 96:d022511.

Hansen K, Näher U. 1999. Evaporation and cluster abundance spectra. Phys Rev A 60:1240.

Hansen K, Stockett MH, Kamińska M, Nascimento RF, Anderson EK, Gatchell M, Chartkunchand KC, Eklund G, Zettergren H, Schmidt HT, Cederquist H. 2017b. Spontaneous decay of small copper-cluster anions $Cu_n^-(n = 3 - 6)$, on long time scales. Phys Rev A 95:022511.

Harvey AJ, Sen A, Yoshikawa N, Dessent CE. 2015. UV laser spectroscopy of mass-selected ionic liquid building blocks in the gas-phase. Chem Phys Lett 634(Suppl C):216–220.

Houston PL, Conte R, Bowman JM. 2014. Collisional energy transfer in highly excited molecules. J Phys Chem A 118:7758–7775.

Ishida T, Murayama T, Taketoshi A, Haruta M. 2020. Importance of size and contact structure of gold nanoparticles for the genesis of unique catalytic processes. Chem Rev 120:464–525.

Ji M, Bernard J, Chen L, Brédy R, Ortéga C, Joblin C, Cassimi A, Martin S. 2017. Cooling of isolated anthracene cations probed with photons of different wavelengths in the Mini-Ring. J Chem Phys 146:044301.

Jinno S, Takao T, Omata Y, Satou A, Tanuma H, Azuma T, Shiromaru H, Okuno K, Kobayashi N, Watanabe I. 2004. TMU electrostatic ion storage ring designed for operation at liquid nitrogen temperature. Nucl Instrum Methods Phys Res A 532:477–482.

Katakuse I, Ichihara T, Fujita Y, Matsuo T, Sakurai T, Matsuda H. 1985. Mass distributions of copper, silver and gold clusters and electronic shell structure. Int J Mass Spectrom Ion Process 67:229–236.

Kaydashev V, Ferrari P, Heard C, Janssens E, Johnston RL, Lievens P. 2016. Optical absorption of small palladium-doped gold clusters. Part Part Syst Char 33:364–372.

King KD, Barker JR. 2019. Comprehensive chemical kinetics, pp. 3–62. Elsevier.

Knight WD, Clemenger K, de Heer WA, Saunders WA, Chou MY, Cohen ML. 1984. Electronic shell structure and abundances of sodium clusters. Phys Rev Lett 52:2141.

Kono N, Suzuki R, Furukawa T, Matsumoto J, Tanuma H, Shiromaru H, Azuma T, Hansen K. 2018. Electronic and vibrational radiative cooling of the small carbon clusters C_4^- and C_6^-. Phys Rev A 98:063434.

Kroto HW, Heath JR, O'Brien SC, Curl RF, Smalley RE. 1985. C_{60}: Buckminsterfullerene. Nature 318:162.

Lange M, Froese M, Menk S, Varju J, Bastert R, Blaum K, Lóopez-Urrutia JRC, Fellenberger F, Grieser M, vonHahn R, Heber O, Kühnel KU, Laux F, Orlov DA, Rappaport ML, Repnow R, Schröoter CD, Schwalm D, Shornikov A, Sieber T, Toker Y, Ullrich J, Wolf A, Zajfman D. 2010. A cryogenic electrostatic trap for long-time storage of keV ion beams. Rev Sci Instrum 81:055105.

Lange M, Froese MW, Menk S, Bing D, Fellenberger F, Grieser M, Laux F, Orlov DA, Repnow R, Sieber T, Toker Y, vonHahn R, Wolf A, Blaum K. 2012. Radiative cooling of Al_4^- and Al_5^- in a cryogenic environment. New J Phys 14:065007.

Lendvay G, Schatz GC. 2019. Comprehensive chemical kinetics, pp. 63–107. Elsevier.

Malpathak S, Hase WL. 2019. Unimolecular rate constants versus energy and pressure as a convolution of unimolecular lifetime and collisional deactivation probabilities. Analyses of intrinsic non-RRKM dynamics. J Phys Chem A 123:1923–1928.

Martin S, Bernard J, Brédy R, Concina B, Joblin C, Ji M, Ortega C, Chen L. 2013. Fast radiative cooling of anthracene observed in a compact electrostatic storage ring. Phys Rev Lett 110:063003.

Martin S, Chen L, Al-Mogeeth A, Bernard J. 2019. Fragmentation and cooling of doubly charged anthracene studied in an electrostatic storage ring. Phys Rev A 99:012712.

Martin S, Ji M, Bernard J, Brédy R, Concina B, Allouche A, Joblin C, Ortega C, Montagne G, Cassimi A, et al. 2015. Fast radiative cooling of anthracene: Dependence on internal energy. Phys Rev A 92:92.

Martin S, Matsumoto J, Kono N, Ji M-C, Brédy R, Bernard J, Cassimi A, Chen L. 2017. Fluorescence decay of naphthalene studied in an electrostatic storage ring, the mini-ring. Nucl Instrum Meth B 408:209–212.

Matsugi A. 2018. Collision frequency for energy transfer in unimolecular reactions. J Phys Chem A 122:1972–1985.

Matsugi A. 2019. Origin of bath gas dependence in unimolecular reaction rates. J Phys Chem A 123:764–770.

Menk S, Das S, Blaum K, Froese M, Lange M, Mukherjee M, Repnow R, Schwalm D, Hahn R, Wolf A. 2014. Vibrational autodetachment of sulfur hexafluoride anions at its long-lifetime limit. Phys Rev A 89:022502.

Milne BF, Kjær C, Houmøller J, Stockett MH, Toker Y, Rubio A, Nielsen SB. 2016. On the exciton coupling between two chlorophyll pigments in the absence of a protein environment: Intrinsic effects revealed by theory and experiment. Angew Chem Int Ed 55(21):6248–6251.

Møller SP. 1997. ELISA, an electrostatic storage ring for atomic physics. Nucl Instr Meth A 394:281.

Näher U, Hansen K. 1994. Temperature of large clusters. J Chem Phys 101:5367.

Najafian K, Pettersson MS, Dynefors B, Shiromaru H, Matsumoto J, Tanuma H, Furukawa T, Azuma T, Hansen K. 2014. Radiative cooling of C_7^-. J Chem Phys 140:104311.

Nakano Y, Enomoto Y, Masunaga T, Menk S, Bertier P, Azuma T. 2017. Design and commissioning of the riken cryogenic electrostatic ring (RICE). Rev Sci Instrum 88:033110.

Niedner-Schatteburg G, Bondybey VE. 2000. FT-ICR studies of solvation effects in ionic water cluster reactions. Chem Rev 100:4059–4086.

Nielsen SB, Lapierre A, Andersen JU, Pedersen UV, Tomita S, Andersen LH. 2001. Absorption spectrum of the green fluorescent protein chromophore anion in vacuo. Phys Rev Lett 87:228102.

O'Connor AP, Becker A, Blaum K, Breitenfeldt C, George S, Göck J, Grieser M, Grussie F, Guerin EA, vonHahn R, Hechtfischer U, Herwig P, Karthein J, Krantz C, Kreckel H, Lohmann S, Meyer C, Mishra PM, Novotny O, Repnow R, Saurabh S, Schwalm D, Spruck K, Kumar SS, Vogel S, Wolf A. 2016. Photodissociation of an internally cold beam of CH^+ ions in a cryogenic storage ring. Phys Rev Lett 116:113002.

O'Connor GD, Chan B, Sanelli JA, Cergol KM, Dryza V, Payne RJ, Bieske EJ, Radom L, Schmidt TW. 2017. Hydrogen-adduction to open-shell graphene fragments: Spectroscopy, thermochemistry and astrochemistry. Chem Sci 8:1186–1194.

Pais A. 1988. Inward bound. New york: Oxford University Press.

Pedersen HB, Svendsen A, Harbo LS, Kiefer HV, Kjeldsen H, Lammich L, Toker Y, Andersen LH. 2015. Characterization of a new electrostatic storage ring for photofragmentation experiments. Rev Sci Instrum 86:063107.

Rahinov I, Toker Y, Hansen K, Schwalm D, Heber O, Zajfman D. 2016. Effect of a localized charge on the structure and stability of Van der Waals Clusters. Eur Phys J D 70:260.

Reinhed P, Orbán A, Rosén S, Thomas RD, Kashperka I, Johansson HAB, Misra D, Fardi A, Brännholm L, Björkhage MH, Cederquist H, Schmidt HT. 2010. Cryogenic kev ion-beam storage in conetrap-a tool for ion-temperature control. Nucl Instrum Methods Phys Res Sect A 621(1–3):83–90.

Robertson SH. 2019. Comprehensive chemical kinetics, pp. 299–361. Elsevier.

Schmidt HT, Eklund G, Chartkunchand KC, Anderson EK, Kamińska M, de Ruette N, Thomas RD, Kristiansson MK, Gatchell M, Reinhed P, Rosén S, Simonsson A, Källberg A, Löfgren P, Mannervik S, Zettergren H, Cederquist H. 2017. Rotationally cold OH^- ions in the cryogenic electrostatic Ion-Beam storage ring DESIREE. Phys Rev Lett 119:073001.

Schmidt HT, Thomas RD, Gatchell M, Rosén S, Reinhed P, Löfgren P, Brännholm L, Blom M, Björkhage M, Bäckström E, Alexander JD, Leontein S, Hanstorp D, Zettergren H, Liljeby L, Källberg A, Simonsson A, Hellberg F, Mannervik S, Larsson M, Geppert WD, Rensfelt KG, Danared H, Paál A, Masuda M, Halldén P, Andler G, Stockett MH, Chen T, Källersjö G, Weimer J, Hansen K, Hartman H, Cederquist H. 2013. First storage of ion beams in the double electrostatic ion-ring experiment: Desiree. Rev Sci Instrum 84(5):055115.

Smith IWM. 1997. Collisional energy transfer, intramolecular vibrational relaxation and unimolecular reactions. J Chem Soc Faraday Trans 93:3741–3750.

Sundén AEK, Goto M, Matsumoto J, Shiromaru H, Tanuma H, Azuma T, Andersen JU, Canton SE, Hansen K. 2009. Absolute cooling rates of freely decaying fullerenes. Phys Rev Lett 103:143001.

Toker Y, Aviv O, Eritt M, Rappaport ML, Heber O, Schwalm D, Zajfman D. 2007. Radiative cooling of Al_4^- clusters. Phys Rev A 76(5):053201.

Toker Y, Rahinov I, Schwalm D, Even U, Heber O, Rappaport ML, Strasser D, Zajfman D. 2012. Blackbody-induced radiative dissociation of cationic SF_6 clusters. Phys Rev A 86(2):023202.

Tomita S, Andersen JU, Gottrup C, Hvelplund P, Pedersen U. 2001. Dissociation energy for C_2 loss from fullerene cations in a storage ring. Phys Rev Lett 87:073401.

Tomita S, Andersen JU, Hansen K, Hvelplund P. 2003. Stability of Buckminsterfullerene, C_{60}. Chem Phys Lett 382:120–125.

Vogel M, Herlert A, Schweikhard L. 2003. Photodissociation of small group-11 metal cluster ions: Fragmentation pathways and photoabsorption cross sections. J Am Soc Mass Spectrom 14(6): 614–621.

von Helden G, van Heijnsbergen D, Meijer G. 2003. Resonant ionization using IR light: A new tool to study the spectroscopy and dynamics of gas-phase molecules and clusters. J Phys Chem A 107:1671–1688.

Weisskopf V. 1937. Statistics and nuclear reactions. Phys Rev 52:295.

Wellman S, Jockusch RA. 2015. Moving in on the action: An experimental comparison of fluorescence excitation and photodissociation action spectroscopy. J Phys Chem A 119:6333.

Wetzel DM, Brauman JI. 1987. Electron photodetachment spectroscopy of trapped negative-ions. Chem Rev 87:607–622.

Willey KF, Robbins DL, Yeh CS, Duncan MA. 1991. Laser photodissociation spectroscopy of mass-selected metal clusters. Faraday Discuss 92:269–277.

Woodhouse JL, Assmann M, Parkes MA, Grounds H, Pacman S, Anderson JC, Worth GA, Fielding HH. 2017. Photoelectron spectroscopy of luciferin and infraluciferin chromophore anions in vacuo: Competing photodetachment, photofragmentation and internal conversion. Phys Chem Chem Phys 19:22711–22720.

Xu S, Gozem S, Krylov AI, Christopher CR, Weber JM. 2015. Ligand influence on the electronic spectra of monocationic copper-bipyridine complexes. Phys Chem Chem Phys 17:31938–31946.

Yao H, Jockusch RA. 2013. Fluorescence and electronic action spectroscopy of mass-selected gas-phase fluorescein, 2',7'-dichlorofluorescein, and 2',7'-difluorofluorescein ions. J Phys Chem A 117(6):1351–1359.

Klavs Hansen, born 1958, received his PhD degree from the Niels Bohr Institute in his native Denmark in 1991, with a thesis on the electronic shells and supershells in metal clusters. His main interests are thermal and quantal effects in gas phase clusters and molecules, including fullerenes. His work is both experimental and theoretical and involves dynamics on time scales from femtoseconds to hours, studied with short pulse lasers, mass spectrometers and electrostatic storage rings. Since 2016 he is professor at Tianjin University and from 2020 also at Lanzhou University, China. He has a senior visiting professorship at KU Leuven, Belgium.